









Article

Fog Detection Based on Meteosat Second Generation-Spinning Enhanced Visible and InfraRed Imager High Resolution Visible Channel

Saverio Teodosio Nilo ^{1,*}, Filomena Romano ¹, Jan Cermak ^{2,3} , Domenico Cimini ^{1,4} , Elisabetta Ricciardelli ¹ , Angela Cersosimo ⁵, Francesco Di Paola ¹ , Donatello Gallucci ¹, Sabrina Gentile ^{1,4}, Edoardo Gherardi ⁶ , Salvatore Larosa ¹ , Ermann Ripepi ¹  and Mariassunta Viggiano ¹ 

¹ Institute of Methodologies for Environmental Analysis, National Research Council (IMAA/CNR), 85100 Potenza, Italy; filomena.romano@imaa.cnr.it (F.R.); domenico.cimini@imaa.cnr.it (D.C.); elisabetta.ricciardelli@imaa.cnr.it (E.R.); francesco.dipaola@imaa.cnr.it (F.D.P.); donatello.gallucci@imaa.cnr.it (D.G.); sabrina.gentile@imaa.cnr.it (S.G.); salvatore.larosa@imaa.cnr.it (S.L.); ermann.ripepi@imaa.cnr.it (E.R.); mariassunta.viggiano@imaa.cnr.it (M.V.)

² Karlsruhe Institute of Technology (KIT), Institute of Meteorology and Climate Research, 76131 Karlsruhe, Germany; jan.cermak@kit.edu

³ Karlsruhe Institute of Technology (KIT), Institute of Photogrammetry and Remote Sensing, 76131 Karlsruhe, Germany

⁴ Centre of Excellence Telesensing of Environment and Model Prediction of Severe events (CETEMPS), University of L'Aquila, 67100 L'Aquila, Italy

⁵ School of Engineering, University of Basilicata, 85100 Potenza, Italy; angela.cersosimo@imaa.cnr.it

⁶ Institute for Archaeological and Monumental Heritage, National Research Council (IBAM/CNR), 85100 Potenza, Italy; edoardo.gherardi@ibam.cnr.it

* Correspondence: saverio.nilo@imaa.cnr.it; Tel.: +39-0971-427500

Received: 30 January 2018; Accepted: 29 March 2018; Published: 1 April 2018



Abstract: In this study, the Meteosat Second Generation (MSG)—Spinning Enhanced Visible and Infrared Imager (SEVIRI) High Resolution Visible channel (HRV) is used in synergy with the narrow band MSG-SEVIRI channels for daytime fog detection. A new algorithm, named MSG-SEVIRI SatFog, has been designed and implemented. MSG-SEVIRI SatFog provides the indication of the presence of fog in near real time and at the high spatial resolution of the HRV channel. The HRV resolution is useful for detecting small scale daytime fog that would be missed in the MSG-SEVIRI low spatial resolution channels. By combining textural, physical and tonal tests, a distinction between fog and low stratus is performed for pixels identified as low/middle clouds or clear by the Classification-MASK Coupling of Statistical and Physical Methods (C-MACSP) cloud detection algorithm. Suitable thresholds have been determined using a specific dataset covering different geographical areas, seasons and time of the day. MSG-SEVIRI SatFog is evaluated against METEOROLOGICAL Aerodrome Reports (METAR) data observations. Evaluation results in an accuracy of 69.9%, a probability of detection of 68.7%, a false alarm ratio of 31.3% and a probability of false detection of 30.0%.

Keywords: fog detection; satellite data; cloud detection; solar reflectance

1. Introduction

Fog is defined as the suspension of water droplets in the air near the surface that causes a reduction of the horizontal ground visibility to less than one kilometre [1,2]. Fog droplets have variable radii roughly between 1 and 40 μm and falling velocity less than 5 cm/s [3]. Fog has important influence on

different aspects of human life. It affects safety (e.g., reduced visibility for road, marine and air traffic), air quality and economy (e.g., traffic delays, reduced solar energy). Concerning the latter, fog indeed plays an important role in photovoltaic (PV) power production fluctuations, since it modifies the balance between direct and diffuse solar irradiance components reaching the PV panels plane. In particular, fog impacts on diffuse horizontal irradiance according to Mie scattering theory since small droplets redirect incident solar radiation in all directions. Hence PV power production varies as a function of fog layer thickness. Research in satellite meteorology has shown that satellite imagery is useful for detecting fog in areas where there are no other observations. Fog detection with satellite imagery still represents a challenge and different approaches can be found in the literature [3–11]. A first method implemented to detect fog and low clouds was the assessment of their different reflectance characteristics compared to that of other clouds in the visible band [4]. One of the most common approaches in satellite fog and low stratus (FLS) detection uses threshold tests on the brightness temperature differences between 10.8 μm and 3.7 μm channels at night [3]. Its theoretical base is that fog droplets produce a lower emissivity at 3.7 μm than at 10.8 μm . The different emissivity causes a sensible brightness temperature difference between the two infrared channels. This “dual-channel different temperature method” was used in [5,6] with the National Oceanic and Atmospheric Administration (NOAA) Advanced Very High Resolution Radiometer (AVHRR) data to detect fog and stratus cloud at night.

This method has been successfully applied to geostationary instruments [7], such as the Geostationary Operational Environmental Satellite Imager (GOES) and the Meteosat Second Generation (MSG)—Spinning Enhanced Visible and Infrared Imager (SEVIRI) [8]. For daytime, in [9] it has been implemented a satellite fog detection scheme (SOFOS) using MSG-SEVIRI infrared and visible (IR/VIS) channels. The requirement for higher spatial resolution led to the development of a pan-sharpening technique for the detection of FLS [10]. In this approach, the 3 km-resolution narrow band channels have been pan-sharpened using the 1 km High Resolution Visible (HRV) channel; a 1 km resolution FLS mask is then derived applying the SOFOS algorithm to the sharpened channels. Fog detection algorithms have also been developed for Moderate Resolution Imaging Spectroradiometer (MODIS) data, for example, through a radiative transfer-based scheme [11]. The main drawback of sensors aboard polar satellites (e.g., AVHRR, MODIS) is their repetition time, limited to few times per day. Over Central Europe only one MODIS satellite passage in the morning and one in the evening are available. Therefore, this paper presents a new algorithm, named SatFog, designed to detect the presence of fog in near real time from MSG-SEVIRI data at the high spatial resolution of the HRV channel. SatFog was developed to account for two main aspects of fog detection at the same time: the retrieval of small valley fog events and the separation of low clouds into fog and low stratus. Particular attention was paid to the detection of fog events occurring in fair weather conditions and inherently stable atmosphere. The paper is organized as follows: Section 2 gives a brief description of the data set used for training and evaluation; Section 3 introduces the SatFog algorithm, while Section 4 presents the evaluation results and an example of algorithm application. Section 5 draws the conclusions and provides hints for future work.

2. Instruments and Data Description

The SEVIRI radiometer is the main payload on board the MSG geostationary satellites, a series of satellites operated by the European Organization for the Exploitation of Meteorological Satellites (EUMETSAT). To date, the series is composed of MSG-1 (Meteosat 8), MSG-2 (Meteosat 9), MSG-3 (Meteosat 10) and MSG-4 (Meteosat 11). SEVIRI, a 50-cm-diameter aperture line by line scanning radiometer, has twelve spectral channels: eleven channels in infrared and visible bands, with a spatial sampling of 3 km and an actual instantaneous field of view of about 4.8 km at the sub-satellite point and one broadband (0.3–1.1 μm) High Resolution Visible channel, with a spatial sampling of 1 km and an actual instantaneous field of view of about 1.67 km at the sub-satellite point. High temporal resolution (15 min), improved signal-to-noise ratio, enhanced spectral characteristics and higher data

storing precision are the major improvements of SEVIRI with respect to previous sensors [12]. In this study both IR/VIS and HRV channels are considered.

The C-MACSP (cloud Classification-MASK Coupling of Statistical and Physical Methods) is a cloud classification/mask algorithm based on MSG-SEVIRI described in [13,14], which builds on the legacy of MACSP [15]. While MACSP only flags SEVIRI pixels as cloudy or clear, C-MACSP gives information about the cloud type and splits the MACSP “high cloud” class in high thin cloud and high thick cloud. Thus, C-MACSP classifies each SEVIRI pixel as cloud-free, low-middle cloud, high thin cloud, high thick cloud, or convective cloud. C-MACSP uses physical, statistical and temporal information to obtain cloud detection and classification. In detail, the non-parametric K-Nearest Neighbour (K-NN) classifier is used both in the C-MACSP statistical and temporal modules. The K-NN classifier uses textural and tonal features estimated in 3-by-3 pixel boxes whose central point is the pixel to be classified. Textural and tonal features characterizing each pixel are extracted from infrared and visible MSG-SEVIRI channels, except from HRV. The statistical algorithm outputs the probabilities that a pixel belongs to the cloud-free and cloudy classes. The physical algorithm is based on a set of multi spectral threshold tests (derived from both measured and simulated clear datasets) applied to each pixel. The brightness temperature tests and the reflectance tests have been chosen on the basis of the different behaviour of clouds at different wavelengths (the tests are listed in Table 2 of [15]). The C-MACSP [13,14] physical algorithm has been updated by adding a new test that considers the brightness temperature difference between the window channel at 10.8 μm and the water vapour channel at 6.2 μm . The training dataset for the C-MACSP statistical algorithm as well as the threshold values for the C-MACSP physical tests have been updated adding a new class for convective clouds. The statistical and physical algorithms run separately and their outputs (probabilities that the pixel belongs to a cloud-free or a cloudy class) are compared. When they agree the pixel is classified accordingly, otherwise the statistical temporal algorithm is applied. The temporal test exploits MSG-SEVIRI high repetition rate and it applies the K-Nearest Neighbour classifier to the tonal and textural features calculated in “temporal” 3-by-3 pixel boxes, where “temporal” means their elements belong to three subsequent MSG-SEVIRI images, acquired at the time of interest, 15 and 30 min before. C-MACSP was evaluated against a test dataset of MSG-SEVIRI pixels visually classified by expert. The visual classification was made by carefully observing the RGB composition of properly chosen MSG-SEVIRI channels. The evaluation analysis shows that C-MACSP classifies high thick clouds, convective clouds and low /middle clouds with an accuracy higher than 95%, 95% and 91%, respectively. The high thin clouds are detected with an accuracy of 87.6% during daytime and night-time over sea and with an accuracy of 85% and 84% during daytime and night-time, respectively, over land.

In order to evaluate the MSG-SEVIRI SatFog algorithm, METeorological Aerodrome Reports (METAR) visibility data are used [16]. METAR coded data are collected in aeronautical weather stations. Data collection can be regular or special. Regular measurements are done at fixed temporal rate (10, 20, 30 or 60 min) while special measurements are taken when it occurs a significantly variation of the weather between two regular reports. For our fog presence verification purpose, we focus on the visibility METAR data. The horizontal visibility is reported in meters using 4 digits. The value 9999 means a horizontal visibility of 10 km or more while the value 0000 indicates a visibility of less than 50 m. Visibility may also be expressed in mile. In this case, the value is followed by the letters SM. The Italian METAR network have both fully and partially automated stations. This means that some METAR stations are supervised by an observer that reports manually some information when it is necessary. Although METAR report can contain the specification about the particular direction in which the visibility measurements have been acquired, in our study we considered only 360° visibility data, with no indication on direction. Since vertical visibility is not always available in the Italian METAR data, it was not considered in this study.

3. MSG-SEVIRI SatFog Monitoring Algorithm

SatFog is an algorithm designed to detect fog presence in near-real time and thus gives indication on its temporal evolution. Based on threshold tests, SatFog relies uniquely on MSG-SEVIRI and no

other ancillary data. SatFog uses the output of C-MACSP cloud detection algorithm and it classifies as low cloud or fog the nine HRV pixels contained in the narrowband pixel identified as low/middle clouds or clear sky by C-MACSP. SatFog works over land in daytime condition, i.e., when solar zenith angle is less than 85° . This because SatFog was developed to improve the estimation of solar energy power production, mainly available over land during daylight hours. The land mask has been derived from the GTOPO30 [17] digital elevation model (DEM). GTOPO30 has a horizontal resolution of 30 arcsec, corresponding approximately to 1 km. The DEM grid has been upscaled at the spatial resolution of the HRV, by averaging the GTOPO30 values falling in each HRV pixel. DEM values greater than zero are selected for the land mask. SatFog algorithm is currently set up to run on a domain size of approximately 600 km (E-W) by 1200 km (N-S), covering the whole Italian peninsula. Here, the Po Valley and the Apennines and Alpine valleys are often affected by fog during autumn and spring, especially in the morning hours, when high-pressure stable condition and thermal inversion near the ground are present. SatFog aims at detecting this kind of fog events, characterized by very sharp boundaries and surrounded by clear sky pixels. SatFog does not take into account the pixels covered by snow/ice or by multi-layered clouds. Currently multi-layered clouds are not classified by C-MACSP. Only the highest cloud layer is classified in the pixel and it could be high thin/high thick cloud (in which case the pixel is automatically not considered by SatFog), or low/middle cloud (in which case the pixel is considered by SatFog). The block diagram giving an overview of SatFog is shown in Figure 1.

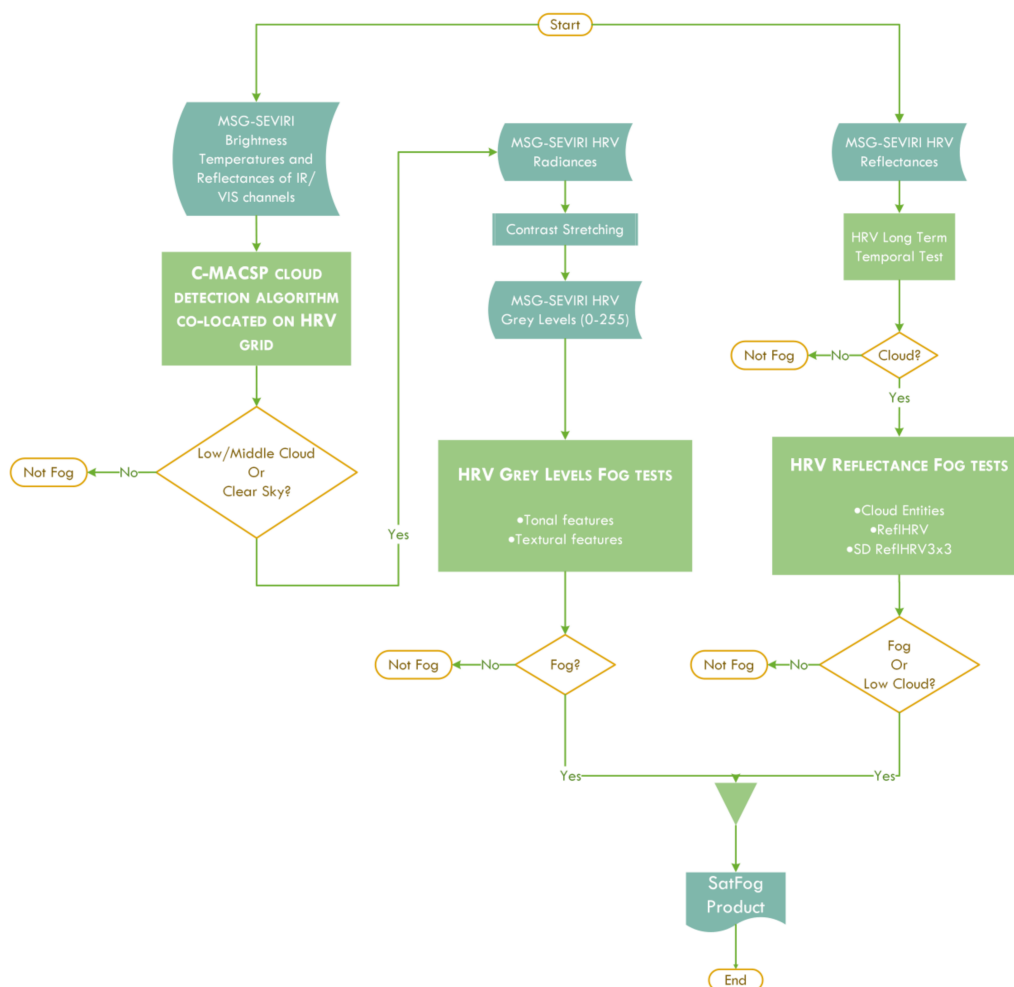


Figure 1. Meteosat Second Generation-Spinning Enhanced Visible and Infrared Imager (MSG-SEVIRI) SatFog algorithm.

The workflow is as follows. The algorithm calls C-MACSP to classify the cloud type at VIS/IR channel resolution and subsequently co-locates its output on HRV grid [18] (left side of Figure 1); henceforth, only low/middle clouds and cloud-free pixels are considered. It should be noticed that cloud-free pixels have to be included because the lower resolution of VIS/IR may hide smaller fog areas that could be otherwise detected by SatFog. In fact, it is possible that one or more of the nine HRV pixels co-located in a cloud-free C-MACSP pixel is not clear. The areas identified as cloud free or low/middle clouds by C-MACSP are further evaluated at HRV spatial resolution on the basis of HRV Grey Levels tests (central part of Figure 1), in order to select those pixels characterized by the presence of fog. The HRV Grey Levels tests are applied to spatial and textural features; these are calculated by using the HRV radiances grey levels after a stretching contrast operation and the relative grey level co-occurrence matrix. Furthermore, HRV Reflectance Fog tests -specifically designed for HRV reflectances- have also been implemented (right side of Figure 1): cloudy pixels are firstly selected by means of HRV Long Term Temporal Test and then linked in homogeneous cloud entities with the Cloud Entities test. Finally, the $Refl_{HRV}$ and the SD $Refl_{HRV_{3 \times 3}}$ tests are applied to the reflectances and their standard deviations (calculated in 3-by-3 boxes) in order to identify among the cloud entities those areas characterized by the presence of fog or low clouds. The pixel classified as fog in all the aforementioned tests are finally flagged as fog and form the SatFog product. It is worth mentioning that suitable thresholds for HRV Grey Level Fog tests (central part of Figure 1) and for HRV Reflectance Fog tests (right side of Figure 1) were retrieved separately. In detail, a manually selected sample dataset was used to determine the thresholds for tonal and textural features tests, while the minimum HRV reflectance over the previous 10 days is used to determine the thresholds for HRV reflectance tests. Both classes of thresholds are dynamical because (i) the tonal and textural features are selected on the basis of the solar and satellite zenith angles and (ii) the HRV reflectance thresholds are calculated for each time slot. The HRV Grey Level Fog tests and the HRV Reflectance Fog tests are described in more detail in Sections 3.1 and 3.3, respectively. The HRV reflectances used in the HRV Reflectance Fog tests are calculated according to the Bidirectional Reflectance Function (BDRF) for the SEVIRI warm channels formula (1)

$$refl_{HRV} = \frac{\pi \cdot rad_{HRV} \cdot d^2(t)}{I_{HRV} \cdot \cos(\vartheta(t, x))} \quad (1)$$

where

- $refl_{HRV}$ is the BDRF for the HRV channel,
- rad_{HRV} is the measured radiance in $mW \cdot m^{-2} \cdot sr^{-1} \cdot (cm^{-1})^{-1}$,
- $d(t)$ is the Sun-Earth distance in Astronomical Unit (AU) at time t ,
- I_{HRV} is the band solar irradiance for the HRV channel at 1 AU in $mW \cdot m^{-2} \cdot sr^{-1} \cdot (cm^{-1})^{-1}$,
- $\vartheta(t, x)$ is the Solar Zenith Angle in Radians at time t and location x .

3.1. HRV Grey Levels Fog Tests

This part includes tonal and textural tests used to classify pixels as fog, low cloud, or clear sky. Tonal and textural features (described in Table 1) can be useful to identify objects in an image. Tonal features are strictly related to the image grey-level appearance and they describe the average tonal variations in a spectral band. Textural features give information about the spatial distribution of tonal variations in a spectral band. Moreover, it is important to select correctly the size of the area for evaluating tonal and textural features in order to prevent one feature from dominating over the other [19]. In this study, a 3×3 box is chosen. We also considered the tonal and textural features determined in 5×5 box but their discriminating power is lower than that of the 3×3 box tonal and textural features. This is because a 5×5 (or higher) box provides information on a wider region, compared to the phenomenon we are interested. The range of textural and tonal characteristics values depends on the object that is observed: clear sky has got low values for contrast and entropy, while tonal features like maximum, minimum and mean strictly depend on spectral band. Generally, the high

optically-thin clouds are characterized by entropy and ASM values lower than those characterizing high optically-thick clouds and higher than those related to low stratus or fog. This is due to the fact that generally high thick/thin clouds are characterized by a highly structured texture while the texture of low stratus and fog is smooth. Because of this, both low stratus and fog are characterized by entropy and ASM values lower than the values related to high thin/thick clouds and thus these features are not so useful for differentiating low stratus from fog. Conversely, on the basis of the Fisher criterion [20,21], the correlation and contrast at 135° and 45° have been chosen to discriminate low stratus from fog. This is supported by the distribution of correlation and contrast from the training set reported in Figure 2. It can be noticed that the values of contrast at 45° and 135° are generally higher for stratus than for fog. The opposite happens, to a lesser extent, for correlation at 135°.

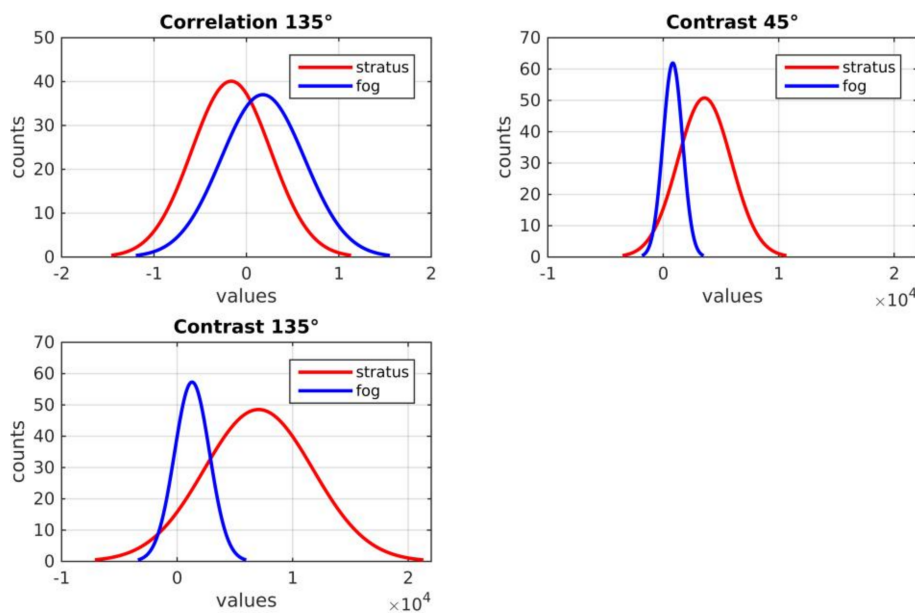


Figure 2. Distributions of textural features selected by the Fisher criterion. Red lines indicate pixels with stratus, blue lines with fog.

Starting from HRV radiances, grey levels quantized with 8 bits have been calculated. Grey levels (gl) are the result of a linear contrast stretching operation (2) applied to the radiance intensity values.

$$gl(x, y) = \frac{rad_{HRV}(x, y) - \min(rad_{HRV})}{\max(rad_{HRV}) - \min(rad_{HRV})} * N_{gl}, \quad (2)$$

where $rad_{HRV}(x, y)$ is the HRV radiance of the pixel located at row x and column y in the HRV grid, $\max(rad_{HRV})$ and $\min(rad_{HRV})$ values are determined for the HRV study area at the time of interest and $N_{gl} = 2^8 = 256$ is the number of all the possible grey levels (gl).

After that, tonal and textural features have been extracted for the 3×3 HRV boxes. The tonal features considered here are the minimum, maximum, mean, standard deviation and median grey levels (the corresponding formulas are reported in Table 1).

Table 1. Tonal and textural features. GLCM stands for Grey Level Co-occurrence Matrix (see main text for details).

Feature	Formula	Description
Minimum	$\min_{3 \times 3}(gl)$	-
Maximum	$\max_{3 \times 3}(gl)$	-
Max Min Ratio	$\frac{\min_{3 \times 3}(gl)}{\max_{3 \times 3}(gl)}$	-
Median	$\text{median}_{3 \times 3}(gl)$	-
Mean	$\mu_{gl} = \frac{1}{N} \sum_{i=1}^N gl_i, N = 8$	-
Standard Deviation	$\sigma_{gl} = \sqrt{\frac{1}{N} \sum_{i=1}^N (gl_i - \mu_{gl})^2}, N = 8$	-
Entropy	$ENT(d, \theta) = - \sum_{i,j} p(i,j) \log_e p(i,j)$	It is a statistical measure of randomness inside an image block. High values occur when all the gl have an equal probability of occurring, while low values reveal a smooth or highly structured texture.
Homogeneity	$HOM(d, \theta) = \sum_{i,j} \frac{p(i,j)}{1+ i-j }$	It gives an indication of the closeness of the distribution of elements in the GLCM to the GLCM diagonal. It is 1 for a diagonal GLCM.
Contrast	$CONTR(d, \theta) = \sum_{i,j} i-j ^2 p(i,j)$	It measures the local variation of GLCM in a grid box 3×3 . It returns a measure of the intensity contrast between a pixel and its neighbours over the whole image. It is 0 for a constant image block.
Correlation	$CORR(d, \theta) = \sum_{i,j} \frac{(i-\mu_i)(j-\mu_j) p(i,j)}{\sigma_i \sigma_j}$	It returns a measure of how correlated a pixel is to its neighbours over the image block. Correlation is 1 or -1 for a perfectly positively or negatively correlated image block. Correlation is not defined for a constant image.
Angular Second Moment	$ASM(d, \theta) = \sum_{i,j} p(i,j)^2$	It measures the homogeneity of the GLCM. It returns the sum of squared elements in the GLCM. It is 1 for a constant image block.

Following [19], a Grey Level Co-occurrence Matrix (GLCM) has been created using neighbouring grey-tone (Figure 3) in order to derive textural features. GLCM gives an indication of the spatial relationship of pixels and characterizes the texture of an image by calculating how often pairs of pixels with specific values and in an unambiguous spatial relationship occur in an image. Specifically, GLCM contains the normalized relative frequency, $p(i, j)$, indicating how often two pixels with grey levels i and j separated by a distance d along the angle θ occur within an image block. The separation distance d has been assumed $d = 1$, while the angle $\theta = 0^\circ, 45^\circ, 90^\circ, 135^\circ$.

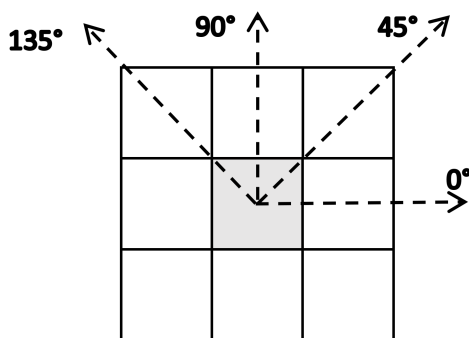


Figure 3. 8- connected Neighbours pixels Grey Level Co-occurrence Matrix.

The textural features considered in this study are entropy, homogeneity, contrast, correlation and angular second moment calculated for the four directions (0, 45, 90, 135°) in the 3 × 3-pixel HRV boxes. The number of features has been reduced since not all proved to be useful for the classification. The criterion chosen for features reduction is the Fisher Distance D_{ijk} [20,21]:

$$D_{ijk} = \frac{|\overline{v_{ij}} - \overline{v_{ik}}|}{(\sigma_{ij} + \sigma_{ik})} \tag{3}$$

where $\overline{v_{ij}}$ is the mean and σ_{ij} is the standard deviation of the feature v_i for samples of class C_j . D_{ijk} quantifies the ability of the variable v_i to differentiate class C_j from class C_k . After the application of Fisher criterion, the selected features are min, max, mean, median grey levels, correlation 135° and contrast 45°, 135°. A positive fog test result is obtained when, considering the value of the i th feature $v_i(x, y)$, the pixel with coordinates (x, y) satisfies this condition $thresh_min_{v_i}^{FOG} < v_i(x, y) < thresh_max_{v_i}^{FOG}$ where $thresh_min_{v_i}^{FOG}$ and $thresh_max_{v_i}^{FOG}$ are, respectively, the minimum and the maximum thresholds for the Fog class. This procedure is applied to the other two classes too. In general, the thresholds used for the HRV Grey Levels Tests are calculated using the dataset of Table 2. For each class of interest (Fog, Low cloud or Clear sky) and, respectively, for each feature described in Table 1, the mean ($mean_{v_i}^{C_j}$) and the standard deviation ($stdev_{v_i}^{C_j}$) have been calculated. Subsequently it has been chosen as $thresh_min_{v_i}^{C_j}$ the difference between the mean and the standard deviation of the feature v_i for the class C_j while as $thresh_max_{v_i}^{C_j}$ the sum of the mean and the standard deviation of the feature v_i for the same class. In detail:

$$thresh_min_{v_i}^{C_j} = mean_{v_i}^{C_j} - stdev_{v_i}^{C_j} \tag{4}$$

$$thresh_max_{v_i}^{C_j} = mean_{v_i}^{C_j} + stdev_{v_i}^{C_j} \tag{5}$$

Dataset Description

The threshold computation is a critical part of this algorithm. In this study, the data used for the threshold definition (Table 2) have been manually selected on the basis of direct observations or the MSG-SEVIRI HRV images not used in algorithm evaluation (Table 3). The test data set was built considering MSG-SEVIRI images collected in different areas at different times in daytime depending

on the presence of fog, which was identified by direct knowledge from in-situ observations and visual inspection of RGB images. In detail, visual inspection has been used by further analysing the HRV pixels classified as low cloud by CMACSP. The HRV higher resolution is very useful in distinguishing stratus from fog. In fact, fog is characterized by sharper and more irregular edges than low stratus ones. Moreover, detecting valley fog is relatively simple because fog edges adapt themselves to the valley profile (or contours). These features have been observed not only in the HRV images but also in the HRV FOG RGB, consisting in a combination of the 1.6 μm channel on blue and of HRV channel on red and green [22]. Since fog dissipates more quickly than stratus, the observation of the temporal behaviour of fog/stratus in HRV images was very useful to distinguish fog from low-stratus pixels. Although the careful visual inspection, the fact that passive satellite measurements do not provide direct information on cloud-base is a limitation in the correct detection of fog. By applying this procedure, both the dataset for the threshold determination and the test dataset were built. The SatFog HRV Grey Level tests thresholds are dynamically determined according to solar and satellite zenith and azimuth angles. Tables 2 and 3 list the scenes used for the training of the HRV Grey Levels Fog tests and the evaluation, respectively. The accuracy (defined as the number R of the correctly classified samples, divided by the total number T of the samples, $A = R/T * 100$) of the test dataset has been calculated for each sample. Accuracy values for the different classes (fog, low/middle clouds and clear sky) are reported in Table 4. The number of samples used for the threshold determination for each class is respectively 509 (fog), 504 (low/middle clouds) and 509 (clear sky). The number of samples used for the accuracy calculation is respectively 270 (fog), 232 (low/middle clouds) and 406 (clear sky).

Table 2. Dataset used for thresholds determination.

MSG-SEVIRI Day	Hours (UTC)	Fog	Low/Middle Clouds	Clear Sky
2016-10-12	07:00		x	
2016-10-12	07:15, 07:45, 08:15		x	x
2016-10-12	10:00, 10:45			x
2016-10-13	06:00		x	
2016-10-13	06:15, 06:45, 07:00	x		x
2016-10-13	07:15, 08:00, 08:15, 08:45, 09:00, 09:15, 09:45, 11:00			x
2016-10-14	06:15			x
2016-10-14	06:45, 07:00, 07:15, 07:45, 08:00	x		
2016-10-14	08:15, 09:00, 09:45			x
2016-10-15	06:15		x	
2016-10-16	06:15, 06:45, 07:00, 07:15, 07:45, 08:00, 08:15	x		
2016-10-17	06:00, 06:15, 06:45, 07:00, 07:15, 07:45, 08:00, 08:15, 08:45, 09:00, 09:15	x		
2016-10-19	06:15, 07:00, 07:45, 08:00, 08:15	x		

Table 3. Scenes used for accuracy calculation.

MSG-SEVIRI Day	Hours (UTC)	Fog	Low/Middle Clouds	Clear Sky
2016-11-20	07:00, 07:15, 07:45, 08:00, 08:15	x	x	x
2016-11-20	08:45, 09:00, 09:15, 09:45		x	x
2016-11-21	07:00, 07:15, 07:45	x		x
2016-11-21	08:00, 08:15	x		
2016-11-21	08:45, 09:00, 09:15, 09:45	x	x	x
2016-11-21	10:00		x	

Table 4. Accuracy of the test dataset.

Classes	Classification Accuracy (%)
Fog	90.74
Low/Middle Clouds	95.68
Clear Sky	97.78

3.2. HRV Long Term Temporal Test

HRV Long Term Temporal Test (LTTT) has been developed to select only cloudy HRV pixel from SEVIRI HRV reflectances. The idea is to select cloudy pixels comparing the observation to a clear sky reference map built from previous 10-day observations at the same time and also to simulated clear sky reflectances. This test is composed by two steps: (i) clear sky reflectance is estimated as the minimum value of reflectance for each pixel in the previous 10 days (6); (ii) the difference between actual reflectance and the clear sky reflectance map (7) is compared with a threshold value. If the difference is larger than the threshold, the pixel is classified as cloudy (8). The threshold was estimated considering both simulated and measured clear sky datasets. The former provides a useful estimate of the threshold value variability around the minimum value calculated from the measured data [23]. Using minimum composites in an operational context can lead to not very accurate results, that is why the suggested approach is the use of radiative transfer model simulations.

$$refl_{HRV,CS} = \min_{te(t_0-10,t_0)} (refl_{HRV}(t)) \quad (6)$$

$$\nabla refl_{HRV,CS} = refl_{HRV} - refl_{HRV,CS} \quad (7)$$

$$\nabla refl_{HRV} > thres_{\nabla refl_{HRV}} \Rightarrow \text{cloudy pixel} \quad (8)$$

Figure 4 shows how the HRV LTTT product is obtained. The HRV reflectances are observed on 2017-04-10 at 07:45 UTC (Figure 4a). In Figure 4b the HRV clear sky reference map is reported. Figure 4c shows the HRV LTTT cloudy areas land product. This approach permits to adapt the HRV LTTT product according to the temporal and spatial variability of the ground and of the atmosphere.

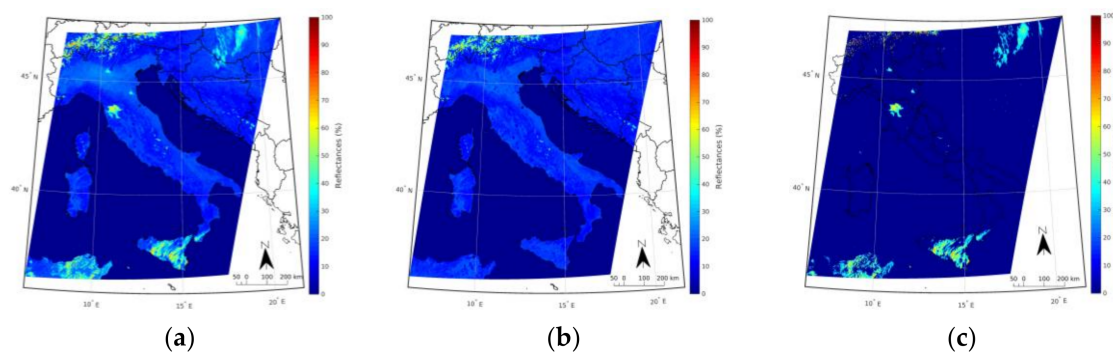


Figure 4. Steps to obtain High Resolution Visible channel (HRV) Long Term Temporal Test (LTTT) product: (a) HRV Reflectance over land, 2017-04-10 07:45 UTC; (b) Clear sky reference map; (c) HRV Reflectance over land, cloudy areas.

To highlight the plausibility of this approach a comparison with the MODIS cloud mask product (MOD35), re-gridded on the MSG-SEVIRI HRV grid is presented. In the literature, MODIS cloud retrieval products are widely used as terms for comparison to evaluate the performances of satellite cloud retrieval products [24–26]. MOD35 is a daily, global Level 2 product generated at 1 km and 250 m (at nadir) spatial resolutions [27]. The algorithm employs a series of visible and infrared threshold and consistency tests to specify confidence that an unobstructed view of the Earth’s surface is observed or not. The re-gridded mask is obtained using the minimum distance criterion between MSG-SEVIRI and MODIS pixel centres, considering that nominally the two products have the same spatial resolution (1 km). As shown in Figure 5, the HRV LTTT produces a cloud mask in agreement with MOD35, though differences are evident in high thin cloud detection. Overall statistical scores are summarized in Table 5.

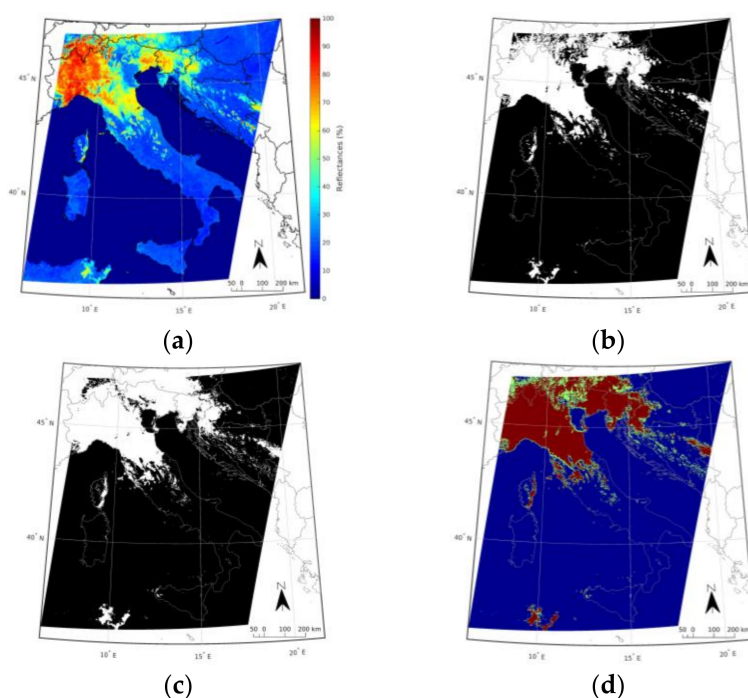


Figure 5. Images comparison between HRV LTTT Cloud Mask and MODIS MOD35 Cloud Mask. MODIS granule pass date 03.03.2017 09:50 UTC, MSG-SEVIRI image date 2017-03-03 09:45 UTC: (a) HRV Reflectance over land; (b) HRV LTTT Cloud Mask; (c) MODIS MOD35 Cloud Mask; (d) differences between HRV LTTT Cloud Mask and MODIS MOD35 Cloud Mask (blue: both clear; red: both cloudy; green: no agreement).

Table 5. Statistical scores of the comparison of the HRV LTTT Cloud Mask with MODIS MOD35 Cloud Mask.

MODIS Granule Pass Date	MSG-SEVIRI Image Date	HRV LTTT Pixels Detected Exactly (%)	Pixels Detected Clear in HRV LTTT but Cloudy in MOD35 Cloud Mask (%)	Pixels Detected Cloudy in HRV LTTT but Clear in MOD35 Cloud Mask (%)
2016-10-13 10:20	2016-10-13 10:15	81.47	15.17	3.36
2016-11-07 10:15	2016-11-07 10:15	84.39	8.64	6.98
2016-11-27 09:50	2016-11-27 09:45	83.52	10.8	5.68
2017-02-18 10:20	2017-02-18 10:15	89.25	6.27	4.48
2017-03-03 09:50	2017-03-03 09:45	91.26	6.07	2.67
2017-04-11 09:55	2017-04-11 09:45	88.79	7.37	3.84
		86.45	9.05	4.5

3.3. HRV Reflectance Fog Tests

This series of tests include Cloud Entities, $Refl_{HRV}$ and $SD\ Refl_{HRV3 \times 3}$ tests. The aim is to locate fog or low stratus areas among the cloudy pixels selected by HRV LTTT. The Cloud Entities test is an object-oriented test. The object-oriented approach aims at the segmentation of the pixels into objects that are related by the same characteristics and permits to treat each object as a whole. In particular we are interested in the segmentation of the different cloud systems present into the domain. In fact, Cloud Entities test returns the connected component according to the 4 connected neighbours method (see Figure 3) [19]. Connected components are regions of adjacent pixels which share the same binary value. The Cloud Entities test provides a segmentation of cloudy areas in different cloud clusters, as shown in Figure 6a in which each detected entity has been represented with a different colour. The $Refl_{HRV}$ test and the $SD\ Refl_{HRV3 \times 3}$ test are entity based threshold tests implemented to identify

cloudy systems characterized by fog or very low clouds. The SD $Refl_{HRV3 \times 3}$ thresholds are estimated using the reference database built with visually identified fog cases (see Table 3). The $Refl_{HRV}$ test aims at selecting those pixels included in minimum ($refl_{HRV,min_thres}$) and maximum ($refl_{HRV,max_thres}$) reflectance thresholds values. In detail:

$$refl_{HRV,min_thres} = refl_{HRV,CS} + D_{min} \quad (9)$$

$$refl_{HRV,max_thres} = refl_{HRV,CS} + D_{max} \quad (10)$$

where the $refl_{HRV,CS}$ is the typical HRV reflectance in clear sky at a certain time calculated as the minimum HRV reflectance over the 10 days before at the same time of the day. This approach takes into account solar and satellite angle variations. The $refl_{HRV,CS}$ is augmented by a pair of fixed values ($D_{min} = 0.15$ and $D_{max} = 0.30$) to obtain the minimum and maximum thresholds values. The 0.15–0.30 range is assumed to account for variations in HRV reflectances due to meteorological variables such as water vapor and temperature.

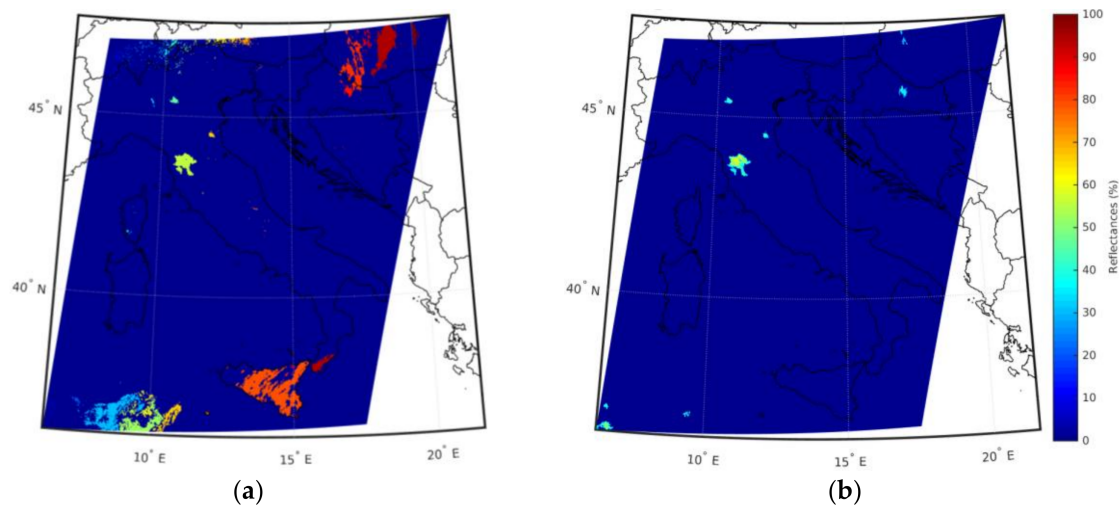


Figure 6. (a) MSG_SEVIRI SatFog Cloud Entities product. Each detected entity has been represented with a different colour. (b) MSG-SEVIRI SatFog final product in which are reported the HRV reflectances of the entities identified as fog by the algorithm proposed.

The presence of a temperature inversion at the fog top is one of the main features that lead to identify fog presence. A temperature inversion inhibits the vertical ascent of the water droplets forcing them to remain in the planetary boundary layer and so to form the fog or stratus layer. The altitude in which the inversion occurs is essential to discriminate fog from stratus. In detail, inversion altitudes lower than 500 m above the surface level should indicate fog presence while inversion altitudes higher than 500 m above the surface level should indicate the stratus presence [11]. The evaluation of the spatial standard deviation of reflectance (SD $Refl_{HRV3 \times 3}$, calculated in 3×3 HRV boxes centred on the pixel of interest) is very useful to discriminate clear sky from fog/low-stratus. By comparing the SD $Refl_{HRV3 \times 3}$ calculated for the clear samples and the fog/low stratus samples of the training dataset, it results that the values of SD $Refl_{HRV3 \times 3}$ associated to clear pixels are higher than that associated to fog/low stratus (SD $Refl_{HRV3 \times 3}$ is 0.4 for clear sky while 0.1 for fog/low stratus). Our findings reveal that SD $Refl_{HRV3 \times 3}$ values lower than dynamical thresholds, determined by taking into account the clear sky SD $Refl_{HRV3 \times 3}$, indicate high probability of having fog/low stratus. This test has to be considered together with the other tests, as shown in the SatFog scheme in Figure 1. An example of the final MSG-SEVIRI SatFog product is the map of fog covered areas shown in Figure 6b.

4. Evaluation Study

4.1. Quantitative Evaluation

Satellite observations offer the undoubted advantage of global coverage for fog detection. However, no adequate ground spatial measurement is available on fog distribution because measurements of visibility and cloud cover are often sparsely distributed. In this study, point horizontal visibility measurements from METAR reports are used as a reference to evaluate the performance of the SatFog algorithm. In particular fog is assumed to be present when the measured visibility is less than 1 km. The evaluation dataset is composed by measurements at eighteen METAR sites in Italy. Forty days, between October 2016 and April 2017, have been considered, selecting observations at morning hours (7 to 11 UTC) for a total sample of 4439 pixels. This period has been chosen because of the high occurrence of fog events. In fact, during fall/winter time, the nights are longer and allow a more significant ground cooling and pronounced temperature inversion that can lead to the fog formation. Considering the notation of the confusion matrix (Table 6), the following categorical statistics have been calculated:

- accuracy (ACC), $ACC = \frac{t_p + t_n}{t_p + t_n + f_p + f_n}$,
- probability of detection (POD), $POD = \frac{t_p}{t_p + f_n}$,
- probability of false detection (POFD), $POFD = \frac{f_p}{f_p + t_n}$,
- false alarm ratio (FAR), $FAR = \frac{f_p}{t_p + f_p}$,
- Hanssen-Kuipers discriminant (HKD), $HKD = POD - POFD$.

Table 6. Confusion matrix, with $t_p = 1466$, $t_n = 1636$, $f_p = 668$, $f_n = 669$.

		SatFog Product	
		True	False
METAR	True	1466	669
	False	668	1636

The quantities t_p , t_n , f_p , f_n are respectively the true positive, true negative, false positive and false negative values used in the confusion matrix (Table 6).

Results obtained for the described categorical statistics are shown in Table 7. SatFog shows good skills in terms of accuracy and probability of detection, while further improvements would be needed to reduce the false alarm ratio and the probability of false detection. To gain further insight, the statistics of the cases incorrectly spotted as fog presence by the algorithm was analysed, finding that 61.4% of these are clear sky cases, whereas the remaining 23.4% and 15.2% feature stratus and partially overcast conditions, respectively. Since comparable performances are found in the literature for a similar product [10], we believe SatFog represents a valid algorithm for fog detection at 1 km of spatial resolution. SatFog has the advantage of displaying fine details of the fog extension that cannot be seen in 3 km spatial resolution product, though it can present cases of false alarm and false detection. False alarms are situations in which SatFog has detected the fog but at ground level METAR data report a high value of visibility. The reason of this is attributable to the presence of very low clouds in the images that SatFog is not able to discriminate but that do not produce a reduction under 1 km of the horizontal visibility. False detections are situations in which the ground visibility is next to 1 km so we are in presence of fog with low optical thickness. In this case SatFog detects clear sky conditions. To put the performance of SatFog into the international context, the statistics may be compared with the scores given by the validation of “GOES-R Advanced Baseline Imager (ABI) Algorithm for Low Cloud and Fog” [28]. It is evident that the statistics of GOES-R ABI algorithm are better than those

given by SatFog. However, in the interpretation of comparison we need to account the following differences between the two algorithms:

- the GOES-R ABI algorithm uses multispectral tests to detect fog/low cloud making no distinction between them, while SatFog mainly uses tests based on the HRV broadband channel to detect fog or low cloud, attempting the distinction between them;
- the two algorithms use observations acquired by different sensors characterized by different spatial resolution (HRV spatial resolution is 1.67 km at the sub-satellite point while ABI measurements are available at 0.5 km, 1 km and 2 km);
- topography of the study area for SatFog (this paper) and GOES-R ABI [28] algorithms is different, the former being characterized by more complex terrain.

One example in which SatFog is able to detect and monitor the fog evolution is reported in the next subsection.

Table 7. MSG-SEVIRI SatFog evaluation scores.

Index	Definition	Score (%)
ACC	$\frac{t_p+t_n}{t_p+t_n+f_p+f_n}$	69.9%
POD	$\frac{t_p}{t_p+f_n}$	68.7%
POFD	$\frac{f_p}{f_p+t_n}$	30.0%
FAR	$\frac{f_p}{t_p+f_p}$	31.3%
HKD	$POD - POFD$	38.7%

4.2. Example of SatFog Application

The proposed example refers to 2017-04-10. In this day stable high pressure, calm wind (as shown in Figure 7) and general clear sky conditions persist all over Italy. The sea level pressure and the wind speed in Figure 7 are taken from ECMWF (European Centre for Medium Range Weather Forecasts) ERA-INTERIM reanalysis with a spatial resolution of 0.125° (about 15 km at mid latitude). Although the horizontal resolution of the reanalysis is much larger than that of SatFog products, the purpose here is just to give a qualitative evaluation of the meteorological conditions that are favourable for fog formation. In these conditions, radiative cooling can lead to the condensation of water vapour after its saturation.

This occurs in the north of Tuscany and in the Po Valley (region highlighted in Figure 7) in the early morning hours where fog has been detected by SatFog algorithm and it was confirmed by direct observation. Figure 8 shows the temperature profile as measured by a radiosonde launched from the San Pietro Capofiume launching station (data available from IGRA, the Integrated Global Radiosonde Archive), the closest radiosonde launching station with respect to the place where fog events occurred.

The presence of the surface inversion in the temperature profile is a proxy for fog formation. Night time radiation loss from earth's surface results in cool temperatures at the surface. Temperature increases rapidly with height since most cooling occurs only at the surface in the lower troposphere (Figure 8). Using the Skew T Log P Diagram, it is possible to infer the surface temperature necessary for the dissipation of fog. The temperature of the dry adiabatic at the surface level is the temperature necessary for dissipation and it is referred to as the critical temperature. In the conditions reported in Figure 8, the T_c is approximately 17 °C (290 K). This value is an approximation, since it assumes stationary conditions from the time of observation to the time of dissipation. The surface temperature increase after sunrise is due to the sun warming the earth's surface and the following convective mixing. So, to infer the timing of fog dissipation, the surface temperature recorded by the station at San Pietro Capofiume (11.61°E; 44.65°N) is reported in Figure 9; the yellow star indicates the critical

temperature, reached approximately at 8:15 UTC. So, we speculate that fog persists until 8–8:30 UTC in San Pietro Capofiume.

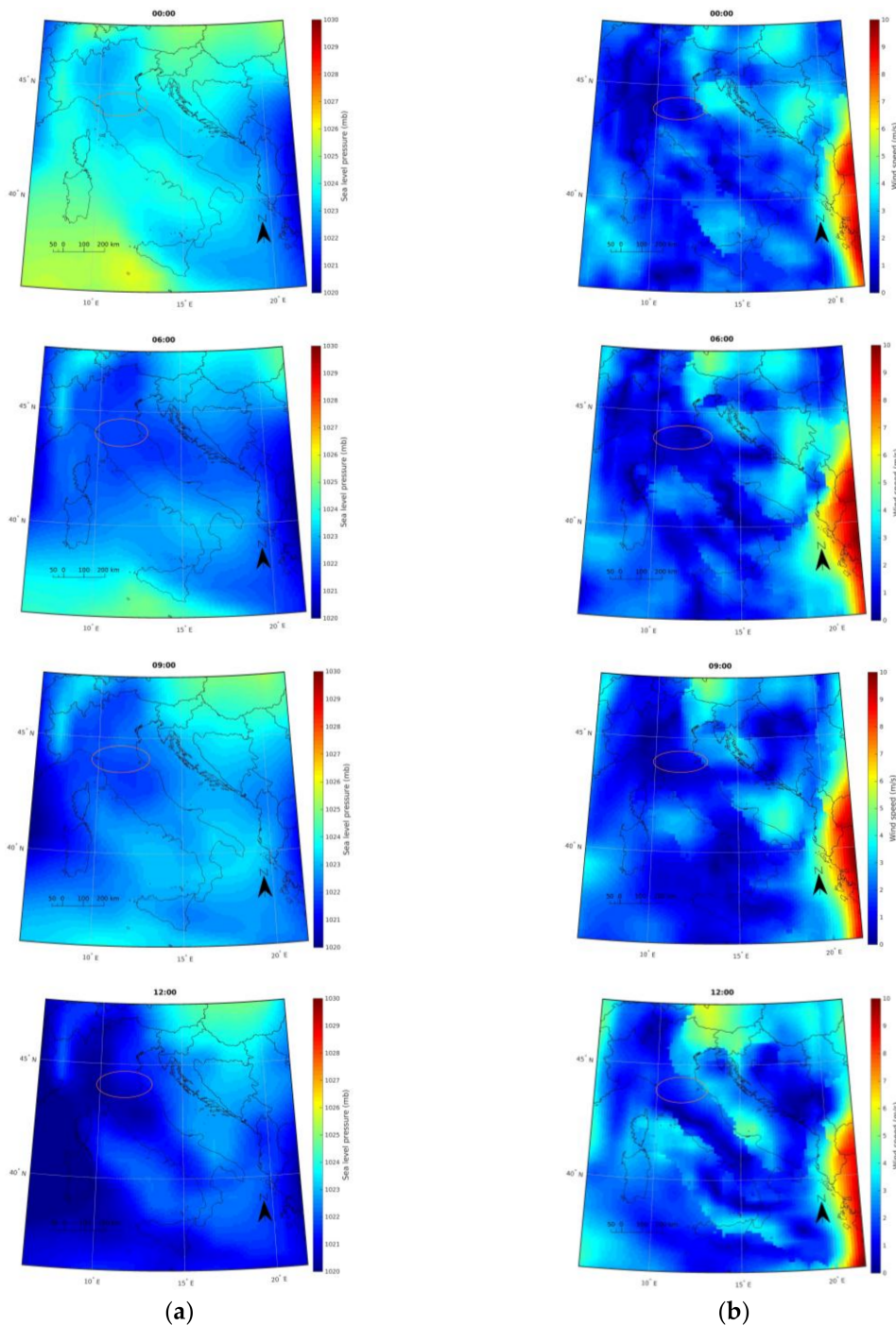
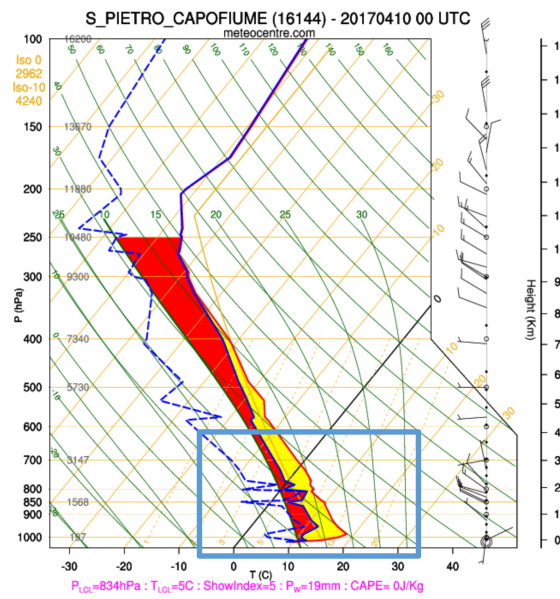
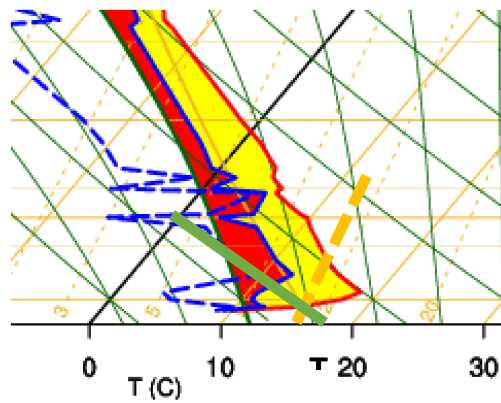


Figure 7. European Centre for Medium Range Weather Forecasts (ECMWF) reanalysis product for 2017-04-10 at 00:00, 06:00, 09:00 and 12:00 UTC: (a) Sea level pressure (mb); (b) Wind speed (ms⁻¹).



(a)



(b)

Figure 8. Skew T Log P diagram and a zoom of the blue rectangular region of the radiosonde launched from San Pietro Capofiume (44.6539°N, 11.6225°E) launching station. Measurement from 2017-04-10 at 00:00 UTC: (a) Skew T Log P diagram between 0 and 16 km altitudes; (b) Zoomed Skew T Log P diagram between 0 and 4 km altitudes.

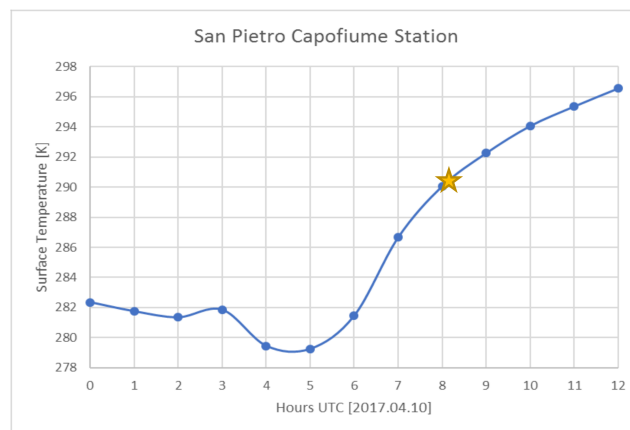


Figure 9. Surface temperature recorded by the station of San Pietro Capofiume (11.61°E; 44.65°N).

For this case study, SatFog has proven to be able to identify fog with a spatial resolution of 1 km at nadir and to follow its evolution until it dissipates. Figure 4a shows the HRV MSG-SEVIRI channel image on 2017-04-10 at 07:45 UTC. Figure 6b shows the fog mask obtained after the application of SatFog algorithm. In Figure 10 the temporal evolution of SatFog product shows its capability to detect and follow the fog dissipation process while Figure 11 is the same temporal evolution of Figure 10 with a focus on the fog spot.

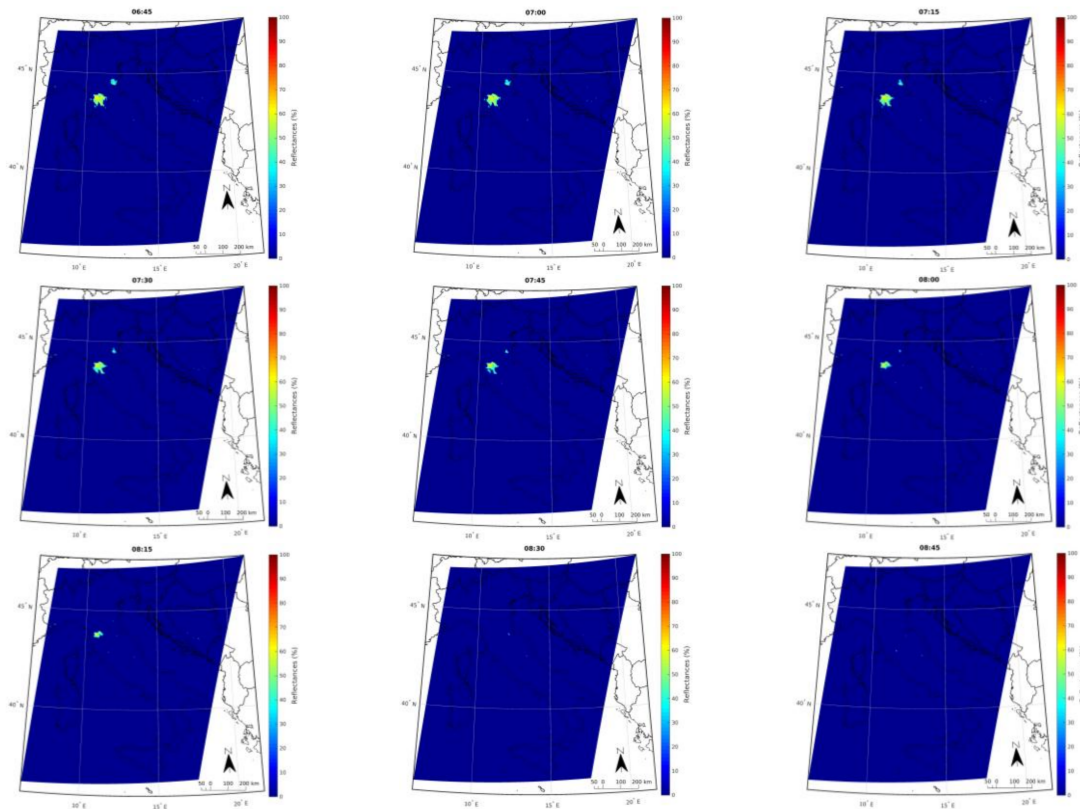


Figure 10. Fog temporal evolution detected by SatFog algorithm on 2017-04-10 between 06:45 and 08:30 UTC.

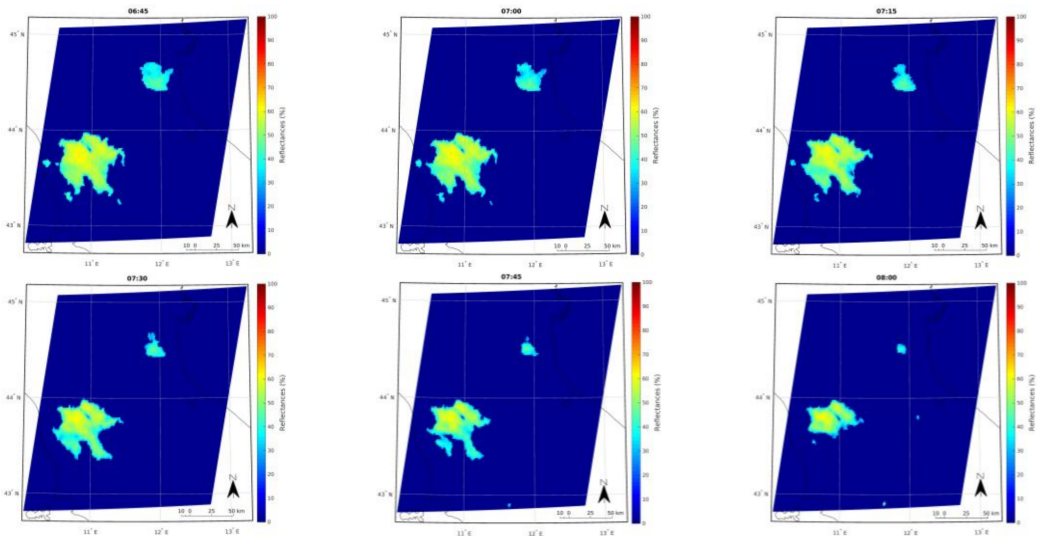


Figure 11. Cont.

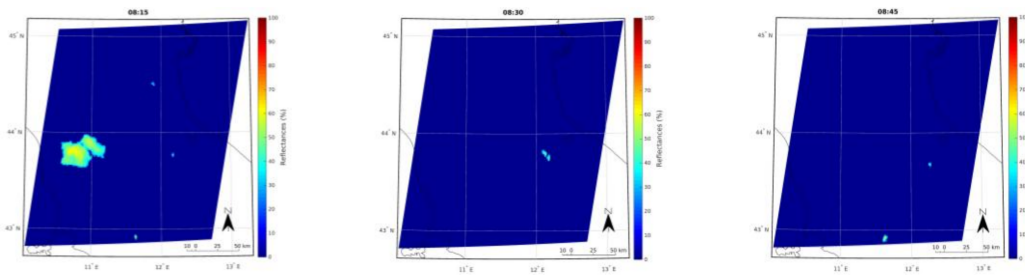


Figure 11. Fog temporal evolution detected by SatFog algorithm on 2017-04-10 between 06:45 and 08:30 UTC. Zoom on the fog spot.

5. Conclusions

This study presents the design and testing of the new algorithm SatFog for detecting daytime fog over land from MSG/SEVIRI geostationary satellite observations, exploiting the synergy of the SEVIRI HRV and lower resolution channels. SatFog algorithm is conceived to detect fog at a nominal spatial resolution of 1 km at nadir and temporal resolution of 15 min. SatFog couples statistical spatial, tonal and textural tests based on the VIS/IR and HRV observations from EUMETSAT MSG/SEVIRI.

SatFog builds on the output of the C-MACSP algorithm for cloud detection and classification from SEVIRI VIS/IR channels. The output of C-MACSP is then regridded at HRV resolution. Pixels classified as low/middle clouds or cloud-free are processed further. Other pixels are flagged as “No fog.” A distinction between fog and low stratus is performed for pixels identified as low/middle clouds or clear by the C-MACSP cloud detection algorithm. Low resolution cloud-free pixels are further investigated to search for fog conditions at HRV resolution. Three layers of tests are applied: (i) the HRV Grey Levels Fog tests, designed to classify the area identified as cloud free or low/middle clouds by C-MACSP; (ii) HRV Long Term Temporal Test, designed to select cloudy HRV pixel from SEVIRI HRV reflectances; and (iii) HRV Reflectance Fog tests, designed to locate fog or low stratus areas among the cloudy pixels selected by HRV LTTT. A current limitation of the SatFog algorithm is that it has been designed for daytime over land detection only.

The performances of SatFog have been evaluated against ground-based METAR data. Evaluation was carried out on a 40-day period (October 2016 to April 2017) with relatively high occurrence of fog events. Only morning hours (7 to 11 UTC) were considered, for a total sample of 4439 pixels. Performances are evaluated in terms of categorical statistics: accuracy (69.9%), probability of detection (68.7%), false alarm ratio (31.3%), the probability of false detection (30.0%) and Hanssen-Kuipers discriminant (38.7%). Comparable performances are found in the literature for other fog techniques at the same spatial resolution. Thus, SatFog represents a valid alternative for daytime fog detection at 1 km spatial resolution over land. For future work, we aim to increase the detection skills and decrease false alarms. For this purpose, we plan to investigate the information content carried by land cover characterization and climate information to improve the performances of SatFog fog retrieval.

Acknowledgments: This work has been financed by the Italian Ministry of Economic Development (MISE) in the framework of the SolarCloud project, contract No. B01/0771/04/X24. Part of this work has been developed in the framework of Short Term Mobility 2017 program funded by the Italian National Research Council.

Author Contributions: Saverio Teodosio Nilo, Filomena Romano, Elisabetta Ricciardelli and Domenico Cimini designed the research, wrote the paper and contributed to evaluation process. Jan Cermak, Francesco Di Paola, Donatello Gallucci, Angela Cersosimo, Edoardo Gherardi, Salvatore Larosa, Sabrina Gentile, Ermann Ripepi and Mariassunta Viggiano contributed to data processing, analysis and evaluation process. All the co-authors helped to revise the manuscript.

Conflicts of Interest: The authors declare no conflict of interest. The founding sponsors had no role in the design of the study; in the collection, analyses, or interpretation of data; in the writing of the manuscript and in the decision to publish the results.

References

1. World Meteorological Organization (WMO). *International Meteorological Vocabulary*, 2nd ed.; Secretariat of the WMO: Geneva, Switzerland, 1992; p. 782.
2. Glickman, T.S. *Glossary of Meteorology*, 2nd ed.; American Meteorological Society: Boston, MA, USA, 2000; p. 855.
3. Gultepe, I.; Tardiff, R.; Michaelides, S.; Cermak, J.; Bott, A.; Bendix, J.; Müller, M.D.; Pagowski, M.; Hansen, B.; Ellrod, G.; et al. Fog research: A review of past achievements and future perspectives. *Pure Appl. Geophys.* **2007**, *164*, 1121–1159. [[CrossRef](#)]
4. Hunt, G.E. Radiative properties of terrestrial clouds at visible and infra-red thermal window wavelengths. *Q. J. R. Meteorol. Soc.* **1973**, *99*, 346–369. [[CrossRef](#)]
5. Eyre, J.R.; Brownscombe, J.L.; Allam, R.J. Detection of fog at night using advanced very high-resolution radiometer. *Meteorol. Mag.* **1984**, *113*, 266–271.
6. Turner, J.; Allam, R.J.; Maine, D.R. A case study of the detection of fog at night using channel 3 and 4 on the advanced very high-resolution radiometer (AVHRR). *Meteorol. Mag.* **1986**, *115*, 285–290.
7. Bendix, J. A fog monitoring scheme based on MSG data. In Proceedings of the 1st MSG RAO Workshop, Bologna, Italy, 17–19 May 2000; ESA SP-452. pp. 131–134.
8. Cermak, J.; Bendix, J. Dynamical night-time fog/low stratus detection based on Meteosat SEVIRI data: A feasibility study. *Pure Appl. Geophys.* **2007**, *164*, 1179–1192. [[CrossRef](#)]
9. Cermak, J.; Bendix, J. A novel approach to fog/low stratus detection using Meteosat 8 data. *Atmos. Res.* **2008**, *87*, 279–292. [[CrossRef](#)]
10. Schulz, H.M.; Thies, B.; Cermak, J.; Bendix, J. 1 km fog and low stratus detection using pan-sharpened MSG SEVIRI data. *Atmos. Meas. Tech.* **2012**, *5*, 2469–2480. [[CrossRef](#)]
11. Bendix, J.; Thies, B.; Nauss, T.; Cermak, J. A feasibility study of daytime fog and low stratus detection with TERRA/AQUA-MODIS over land. *Meteorol. Appl.* **2006**, *13*, 111–125. [[CrossRef](#)]
12. Schmetz, J.; Pili, P.; Tjemkes, S.; Just, D.; Kerkmann, J.; Rota, S.; Ratier, A. An Introduction to Meteosat second generation (MSG). *Bull. Am. Meteorol. Soc.* **2002**, *83*, 977–992. [[CrossRef](#)]
13. Ricciardelli, E.; Cimini, D.; Di Paola, F.; Romano, F.; Viggiano, M. A statistical approach for rain intensity differentiation using Meteosat second generation-spinning enhanced visible and infrared imager observations. *Hydrol. Earth Syst. Sci.* **2014**, *18*, 2559–2576. [[CrossRef](#)]
14. Di Paola, F.; Ricciardelli, E.; Cimini, D.; Romano, F.; Viggiano, M.; Cuomo, V. analysis of Catania flash flood case study by using combined microwave and infrared technique. *J. Hydrometeorol.* **2014**, *15*, 1989–1998. [[CrossRef](#)]
15. Ricciardelli, E.; Romano, F.; Cuomo, V. Physical and statistical approaches for cloud identification using Meteosat second generation-spinning enhanced visible and infrared imager data. *Remote Sens. Environ.* **2008**, *112*, 2741–2760. [[CrossRef](#)]
16. ASOS Program Office Staff. *Automated Surface Observing System Users Guide*; National Weather Service ASOS Program Office: Silver Spring, MD, USA, 1998.
17. United States Geological Survey (USGS). *Digital Elevation Models. Data Users' Guide 5*; U.S. Geological Survey: Reston, VA, USA, 1993; p. 48.
18. Romano, F.; Cimini, D.; Rizzi, R.; Cuomo, V. Multilayered cloud parameters retrievals from combined infrared and microwave satellite observations. *J. Geophys. Res.* **2007**, *112*. [[CrossRef](#)]
19. Haralick, R.M.; Shanmugan, K.; Dinstein, I. Textural Features for Image Classification. *IEEE Trans. Syst. Man Cybern.* **1973**, *SMC-3*, 610–621. [[CrossRef](#)]
20. Ebert, E. A pattern recognition technique for distinguishing surface and cloud types in the polar regions. *J. Clim. Appl. Meteorol.* **1987**, *26*, 1412–1427. [[CrossRef](#)]
21. Parikh, J. A comparative study of cloud classification techniques. *Remote Sens. Environ.* **1977**, *6*, 67–81. [[CrossRef](#)]
22. Jasiński, J.; Krawczyk, K.; Pietrek, S. Fog detection over sea based on multispectral analysis of satellite images. *Zeszyty Naukowe/Akademia Morska w Szczecinie* **2012**, *29*, 53–62.
23. Romano, F.; Cimini, D.; Nilo, S.T.; Di Paola, F.; Ricciardelli, E.; Ripepi, E.; Viggiano, M. The role of emissivity in the detection of arctic night clouds. *Remote Sens.* **2017**, *9*, 406. [[CrossRef](#)]

24. Geraldi, E.; Romano, F.; Ricciardelli, E. An Advanced Model for the Estimation of the Surface Solar Irradiance Under All Atmospheric Conditions Using MSG/SEVIRI Data. *IEEE Trans. Geosci. Remote Sens.* **2012**, *50*, 2934–2953. [[CrossRef](#)]
25. Hocking, J.; Francis, P.N.; Saunders, R. Cloud detection in Meteosat second generation imagery at the Met Office. *Meteorol. Appl.* **2011**, *18*, 307–323. [[CrossRef](#)]
26. Bley, S.; Deneke, H. A threshold-based cloud mask for the high-resolution visible channel of Meteosat second generation SEVIRI. *Atmos. Meas. Tech.* **2013**, *6*, 2713–2723. [[CrossRef](#)]
27. Ackerman, S.; Strabala, K.; Menzel, W.P.; Frey, R.A.; Moeller, C.C.; Gumley, L.E. Discriminating clear sky from clouds with MODIS. *J. Geophys. Res.* **1998**, *103*, 141–157. [[CrossRef](#)]
28. Calvert, C.; Pavolonis, M. *GOES-R Advanced Baseline Imager (ABI) Algorithm Theoretical Basis Document for Low Cloud and Fog*; NOAA NESDIS Centre for Satellite Applications and Research: College Park, MD, USA, 2010; p. 77.



© 2018 by the authors. Licensee MDPI, Basel, Switzerland. This article is an open access article distributed under the terms and conditions of the Creative Commons Attribution (CC BY) license (<http://creativecommons.org/licenses/by/4.0/>).